Available online at www.sciencedirect.com

SCIENCE DIRECT®

Remote Sensing of Environment 92 (2004) 158–172

Remote Sensing of Environment

www.elsevier.com/locate/rse

Lidar remote sensing for modeling gross primary production of deciduous forests

Svetlana Y. Kotchenova[a,*], Xiangdong Song[a], Nikolay V. Shabanov[a], Christopher S. Potter[b], Yuri Knyazikhin[a], Ranga B. Myneni[a]

[a] *Department of Geography, Boston University, 675 Commonwealth Avenue, #457, Boston, MA, 02215, USA*
[b] *Ecosystem Science and Technology Branch, NASA Ames Research Center, Moffett Field, CA, USA*

Received 10 October 2003; received in revised form 19 May 2004; accepted 24 May 2004

Abstract

The influence of foliage vertical distribution on vegetation gross primary production (GPP) is investigated in this study. A new photosynthesis model has been created that combines the standard sunlit/shaded leaf separation (two-leaf) and the multiple layer approaches and uses vertical foliage profiles measured by SLICER (the Scanning Lidar Imager of Canopies by Echo Recovery). Daily gross carbon assimilation rates calculated by this model were compared with the rates calculated by two other models, the two-leaf model and the combined two-leaf multilayer model utilizing uniform foliage profiles. The comparison was made over a wide range of profiles and weather conditions for two mixed deciduous forest stands in eastern Maryland, measured by SLICER in September 1995. Incident radiation pattern, environmental parameters and total amounts of sunlit and shaded leaves were the same for all three models. The difference was in the distributions of radiation and sunlit/shaded leaves inside the canopy. For the combined models, these distributions were calculated based on the vertical foliage profiles, while for the two-leaf model, empirical equations were used to account for the average amounts of absorbed radiation. The simulations showed that: (1) the use of a uniform foliage distribution instead of the actual one results in large differences in the calculated GPP values, up to 46.4% and 50.7% for the days with partial and total cloud cover; (2) the performance of the two-leaf model is extremely sensitive to the absorbed radiation pattern, its disagreement with the proposed model becomes insignificant when the average amounts of absorbed radiation are the same; (3) days with partial cloud cover and a greater fraction of diffuse radiation are characterized by higher GPP rates. These findings highlight the importance of vertical foliage profile and separate treatments of diffuse and direct radiation for photosynthesis modeling.

Keywords: Photosynthesis model; Vertical foliage profiles; Lidar remote sensing

1. Introduction

Photosynthetic accumulation of carbon by plants, also known as gross primary production (GPP), is an important component of the terrestrial carbon cycle. Globally, forest plants absorb about 15 P gC/year (IPCC, 2001). Approximately half of this amount is incorporated into new plant tissues such as leaves, roots, and wood, and the other half is released back to the atmosphere through autotrophic respiration.

The traditional approaches to GPP calculation, widely used at regional and global scales, include (1) correlation of GPP with the remotely sensed fraction of photosynthetically active radiation (FPAR) absorbed by vegetation (Heinsch et al., 2003; Potter et al., 1993; Ruimy et al., 1996) and (2) the use of a so-called big leaf model, in which GPP is calculated for one individual leaf at the top and then scaled to the whole canopy (Hunt et al., 1996; Sellers et al., 1992). Both methods are an approximation as per comparisons to field measurements at hourly and daily time steps (Chen et al., 1999; Spitters, 1986).

A sunlit-shaded leaf separation approach, within which the vegetation is treated as two big leaves under different illumination conditions, is gradually replacing the big-leaf strategy, for applications at local and regional scales. A saturating response of leaf photosynthesis to increasing light

* Corresponding author. Tel.: +1-617-353-8843; fax: +1-617-353-8399.
E-mail address: skotchen@bu.edu (S.Y. Kotchenova).

0034-4257/$ - see front matter © 2004 Elsevier Inc. All rights reserved.
doi:10.1016/j.rse.2004.05.010

intensity has long been recognized by the ecological community (Farquhar & Roderick, 2003). It is often found that, under clear sky conditions, the sunlit leaf photosynthetic rate is controlled by temperature and the shaded leaf rate by radiation. The leaf-separation model has been shown to be more accurate in simulating the actual photosynthetic rate compared to the big-leaf strategy (Chen et al., 1999; Wang & Leuning, 1998). This model, however, fails to account for the varying rate of photosynthesis inside the canopy due to the attenuation of incident radiation with height, as it uses the average values of diffuse and direct radiation absorbed by sunlit and shaded leaves. This issue can be addressed by a multilayer formulation.

Within a multilayer model, photosynthesis is estimated separately for each layer based on the amount of photosynthetically active radiation (PAR, 400–700 nm) absorbed by leaves in this layer. This approach requires knowledge of the distribution of foliage with height. Ground measurements of vertical foliage distribution are expensive, time-consuming, and difficult to repeat, and thus are limited to small areas. A standard simplifying assumption is that each layer contains an equal fraction of total leaf area. The multilayer models are in general considered to be less effective in improving GPP estimations as compared to the two-leaf models. Despite their ability to represent the radiation gradient, they fail to capture the effects of light saturation, which are important for sunlit leaves, and light constraint, which define the rate of carbon accumulation for shaded leaves. It has been shown that ignoring the leaf separation may lead to a significant overestimation of canopy photosynthesis (De Pury & Farquhar, 1997, 1999; Spitters, 1986).

The combination of leaf-separation and multilayer approaches (hereafter referred to as the coupled model) is a third potential alternative to the big-leaf strategy. The WIMOVAC model (Windows Intuitive Model of Vegetation response to Atmosphere and Climate change) for simulating canopy microclimate water, and CO_2 exchange over a diurnal, weekly and annual time course is an example of such a coupled model (Humphries & Long, 1995). However, WIMOVAC uses only uniform foliage distributions calculated based on ground-measured values of leaf area index (LAI).

The development of large-footprint waveform-recording laser altimeters has enabled accurate measurements of vertical canopy structure from space. The group includes two air-borne instruments, the previously used Scanning Lidar Imager of Canopies by Echo Recovery (SLICER) (Harding et al., 2000) and the presently used Laser Vegetation Imaging Spectrometer (LVIS) (Blair et al., 1999), which were designed specifically for vegetation sampling, and the space-borne Geoscience Laser Altimeter System (GLAS), launched in January 2003 onboard the ICESat satellite, designed to provide information on ice sheets, clouds and surface elevation along with the measurements of vegetation structure (Zwally et al., 2002).

These light detection and ranging (lidar) instruments operate based on a similar general scheme. A short-duration laser pulse is sent from the zenith to nadir, then the elapsed time between the emission of the pulse and the arrival of the reflection is precisely measured, and the amplitude of reflected energy is recorded as a function of time. The time units are converted into distance to obtain the distribution of intercepted surfaces with height, referred to as the lidar waveform. The last discrete peak of the signal is identified as the ground return.

Distributions of canopy material with height, or canopy height profiles (CHPs), can be retrieved from lidar waveforms (Harding et al., 2001). Until now, the use of CHPs has been mostly limited to aboveground biomass estimations (e.g., Lefsky et al., 1999; Lefsky et al., 1999; Drake et al., 2002) and calculations of the distributions of transmitted direct light inside the canopy given that the source of illumination is directed from the zenith (Parker et al., 2001). Another potential use of lidar measurements of CHPs is for GPP estimations.

To our knowledge, there is not enough evidence in the published literature that the coupled model with uniform foliage profiles provides more accurate estimates of photosynthesis compared to the two-leaf model. In this study, we will test the performance of the both models against the coupled model utilizing CHPs measured by SLICER, under different environmental conditions.

2. Data description

2.1. SLICER data

SLICER data used in this work were collected on September 7, 1995, over two deciduous forest stands located near the Smithsonian Environmental Research Center (SERC, 38°53′ N, 76°33′ W), about 10 km south–southeast of Annapolis, MD, on the western shore of Chesapeake Bay (Harding et al., 2001). The details of SLICER geometry are well covered in Lefsky et al. (1999) and Harding et al. (2000). The measured stands belong to the tulip poplar association, a mixed-deciduous forest with the overstory predominantly comprised of tulip poplar. The other species include sweet gum, oak, hickory, and American beech. This association is most common in the coastal plains and much of the piedmont of mid-Atlantic North America (Lefsky et al., 1999). The stands represent distinct stages in canopy development. An intermediate-aged stand is about 41 years old. It comprises of 14 different woody species and is characterized by a broad unimodal overstory of up to 30 m in height and a slight understory. A mature 99-year-old stand has a bimodal canopy structure with the maximum height of 36 m and comprises of 19 species. The trees were fully foliated at the time of measurements (Harding et al., 2001). The average field estimates of LAI were 5.16 for the intermediate stand and 5.26 for the mature.

Raw SLICER signals were processed following the procedure described in Harding et al. (2001). The main steps include background noise removal, smoothing the signals by calculating the average of three adjacent bins, and identification of the ground return (Fig. 1a,b). The vertical resolution of a SLICER waveform is 0.11 m. SLICER signals are always smoothed during the processing to improve the signal-to-noise ratio. For example, Harding et al. (2001) summed six adjacent bins and used a resolution of 0.33 m. In our study, three bins were enough to get a relatively smooth signal. Signals with no apparent ground return were discarded. Canopy height profiles were calculated using modified MacArthur and Horn's (1969) method as described in Lefsky et al. (1999). The mathematical explanation can be found in Ni-Meister et al. (2001). Three assumptions are required for the application of this method: (1) horizontal distribution of leaves is uniform; (2) multiply scattered photons do not make any significant contribution into the return signal; and (3) CHP can be used as a substitution for the foliage height profile (FHP).

However, the retrieved CHP is different from the actual foliage profile. What can be retrieved from a lidar waveform is a vertical distribution of nadir-intercepted surfaces. According to Ni-Meister et al. (2001), the retrieved and the actual foliage profiles are related as

$$\mathrm{FHP}_{\mathrm{retr}}(z) = \mathrm{FHP}_{\mathrm{act}}(z) \cdot G(z, \theta_{\mathrm{L}}), \tag{1}$$

where $G(z,\theta_{\mathrm{L}})$ is the mean projection of leaf normals on the direction of laser beam θ_{L} at height z (Ross, 1981), and $\mathrm{FHP}_{\mathrm{act}}(z)$ is the foliage area volume density ($\mathrm{m}^2/\mathrm{m}^3$).

In this study, a different approach will be used to obtain actual foliage profiles. The retrieved CHPs will be normalized with the canopy area index (CAI) values, which are assumed to be approximately equal to the total canopy field-measured LAIs (Fig. 1c). The mathematical explanation can be found in Appendix A. The approach proposed by Ni-Meister et al. (2001) leads sometimes to unlikely large LAI values. We suspect that it is related to the inclusion of the contribution of non-foliar surfaces.

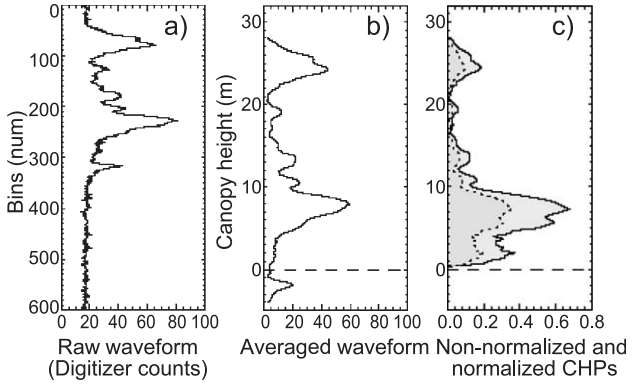

Fig. 1. Processing of SLICER waveforms. (a) Raw SLICER signal measured over the mature stand. One bin corresponds to 0.11 m. (b) Smoothed SLICER signal. Background noise is removed. Digitizer bins are converted into height units. The start of the ground return is identified (dashed line). (c) Non-normalized (CAI = 2.77, dotted line) and normalized (CAI = 5.26) canopy height profiles.

2.2. Meteorological data

Estimation of photosynthesis requires knowledge of ambient environmental parameters such as incident PAR, air temperature, humidity, and wind speed. These data were available from two research stations located in proximity to the SERC forest. The Wye Research and Education Center (38°55′ N, 76°09′ W) provides measurements of incident radiation, temperature and humidity at 3-min time-step (WWW 1). Measurements were taken as part of the USDA UV-B Monitoring and Research Program led by the Natural Resource Ecology Laboratory of Colorado State University. The Andrews AFB station (38°49′ N, 76°52′ W) provides data of daily mean wind speed values (WWW 2). Unfortunately, no other measurements of wind speed were available. The Wye station records start only from 1997, while SLICER records were collected in 1995. We ignore the small dynamic growth during the 2-year period as the forest stands were relatively old.

3. Photosynthesis modeling

In the two-leaf model, the total canopy photosynthesis (A) is calculated as the sum of sunlit and shaded leaf contributions (Norman, 1980):

$$A = A_{\mathrm{sun}} L_{\mathrm{sun}} + A_{\mathrm{shade}} L_{\mathrm{shade}}, \tag{2}$$

where A_{sun} and A_{shade} are the gross photosynthetic rates for unit sunlit and shaded leaf areas, and L_{sun} and L_{shade} are sunlit and shaded LAIs. In the coupled model, with both uniform and retrieved CHPs, photosynthesis will be estimated separately for sunlit and shaded leaves within each layer and then integrated over the whole canopy:

$$A = \sum_{i=1}^{N} A_{\mathrm{layer}}(h_i) = \sum_{i=1}^{N} [A_{\mathrm{sun}}(h_i) L_{\mathrm{sun}}(h_i) + A_{\mathrm{shade}}(h_i) L_{\mathrm{shade}}(h_i)]. \tag{3}$$

The incident radiation pattern, photosynthetic rate of a unit leaf area, total canopy area indices, and total amounts of sunlit and shaded leaves will be the same for a particular CHP in all three models. The coupled model with uniform and actual CHPs will utilize different vertical distributions of radiation and sunlit/shaded leaves. The two-leaf model will utilize empirically corrected radiative transfer equations to calculate the average amounts of direct and diffuse PAR incident on a unit leaf area.

3.1. Radiation pattern

3.1.1. The coupled model radiation pattern

The amounts of diffuse and direct radiation absorbed within each layer were calculated using a multilayer radiative transfer model developed for heterogeneous vegetation canopies by Shabanov et al. (2000). This model is based on the stochastic radiative transfer equation, which is solved numerically by the method of successive orders of scattering approximations. The quality of model simulations was assessed by comparison to field data from shrub lands.

In this study, input variables of the model include: (1) characteristics of solar radiation: zenith and azimuth angles of the direct beam, total incident radiation flux, and direct-to-total incident flux ratio; (2) canopy structural parameters: vegetation height, thickness of one layer, leaf normal orientation distribution, vertical distribution of foliage (FHP), and clumping index β as defined in Chen et al. (1997); (3) optical properties of leaves and soil.

(1) Diffuse (R_{dif}), direct (R_{dir}), and total (R_{total}) fluxes of incident PAR were measured (W m^{-2}) at four different wavelengths (415, 500, 610, and 665 nm) with a multifilter rotating shadow-based radiometer (MFRSR, Yankee Environmental Systems, US; Harrison et al., 1994). The direct-to-total incident flux ratio, f_{dir}, is calculated for each wavelength, λ, as

$$f_{\mathrm{dir}}(\lambda) = \frac{R_{\mathrm{dir}}(\lambda)\cos(\theta)}{R_{\mathrm{total}}(\lambda)}, \tag{4}$$

where θ is the solar zenith angle, which is a function of latitude, day, and time (Rosenberg et al., 1983). The time resolution of the radiation model was set to 30 min and each 10 successive measurements of PAR were summed to produce a half-hour average.

(2) Canopy height is extracted from a SLICER waveform as the distance between the start points of vegetation return and ground peak. The thickness of each layer corresponds to the resolution of an averaged waveform, i.e., $\Delta h = 0.33$ m. The leaf angular distribution is assumed to be uniform. Retrieved CHPs are used as substitutions for FHPs. To obtain a uniform vertical distribution, total CAI is divided by the number of layers. The assumption of a uniform horizontal distribution of leaves means the absence of clumping, i.e., $\beta = 1$ (Chen et al., 1997).

(3) The leaf transmittance and reflectance spectrum of American beech, one of the species from the study site, has been used as an average leaf spectrum for the selected stands. This spectrum was measured as reported in Shabanov et al. (2003). The use of the spectrum of one species instead of the average spectrum of all the species present in the stand will possibly introduce only minor errors in the calculation of the distribution of absorbed energy, as the spectra of most deciduous species are similar. The ground surface, which consisted dominantly of leaf-litter with some bare soil and live foliage elements (Harding et al., 2001), was assumed to be totally absorbing. As the both forest stands are relatively dense and the reflectance of leaf litter is relatively low (Shabanov et al., 2003), the amount of PAR penetrating through the whole vegetation canopy and reflected by the ground surface is negligible.

Vertical distributions of absorbed diffuse and direct PAR, simulated for 2 p.m., August 9th (clear sky conditions) and August 20th (total overcast), 1997, are shown in Fig. 2a and b, respectively, for both the retrieved (Fig. 1c) and the uniform CHPs. The amounts of absorbed PAR were calculated separately for each wavelength and then summed within each layer. The simulations show strong relationship between the absorbed PAR and the form of CHP. For the uniform profile, the amount of absorbed PAR exponentially decreases with height, while for the non-uniform profile significant variations of absorbed PAR, correlated with the variations of foliage density, are evident.

3.1.2. The two-leaf model radiation pattern

For our two-leaf model, we adopted equations used in Guenther et al. (1995). The mean sunlit leaf irradiance (I_{sun}) is calculated as

$$I_{\mathrm{sun}} = R_{\mathrm{dir}}\cos\alpha/\cos\theta + I_{\mathrm{shade}}, \tag{5}$$

where α is the mean leaf-sun angle, which is 60° for a canopy with a uniform leaf angular distribution, and I_{shade} is the mean shaded leaf irradiance. I_{shade} originates from sky irradiance and multiple scattering of direct beam radiation inside the canopy:

$$I_{\mathrm{shade}} = R_{\mathrm{dif}}\exp(-0.5 \cdot \mathrm{LAI}^{0.7}) + 0.07R_{\mathrm{dir}}(1.1 - 0.1\mathrm{LAI})\exp(-\cos\theta). \tag{6}$$

Eq. (6) is slightly different from the equation for I_{shade} used by Chen et al. (1999) for their two-leaf model. Chen et al. (1999) modified this equation to include the influence of clumping and calculate the diffused radiation more accurately. However, in the absence of clumping, the replacement of Eq. (6) with that from Chen et al. does not lead to any significant changes in the results.

3.2. Sunlit and shaded leaves

Equations for estimation of the fraction of sunlit and shaded leaves were developed by Norman (1980). The sunlit and shaded leaf area indices for a layer with

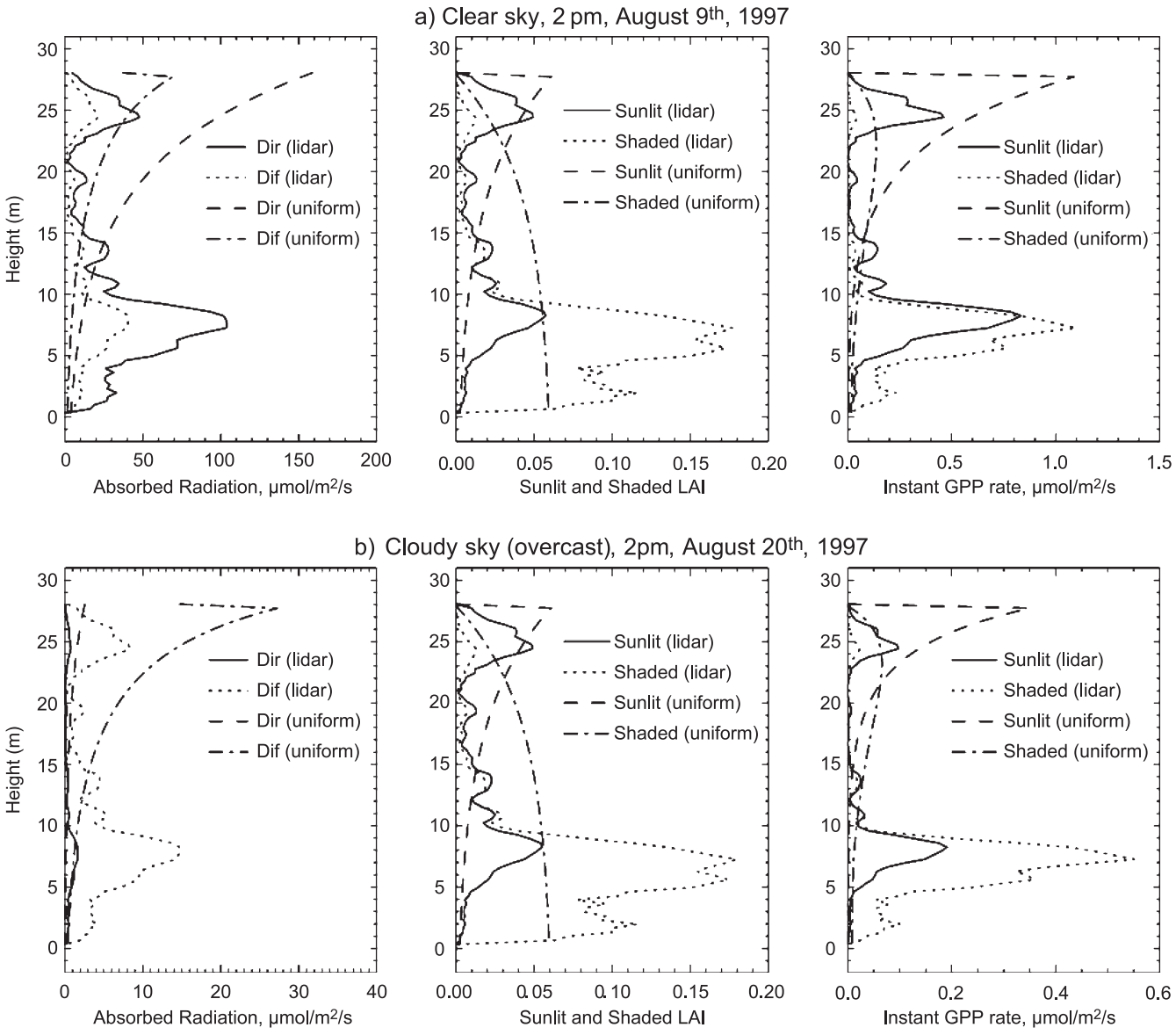

Fig. 2. Diffuse and absorbed PAR, sunlit and shaded LAIs, and instant GPP rates of sunlit and shaded leaves as functions of height for the uniform and the SLICER-measured CHPs, under clear and cloudy sky conditions. The simulations are made for 2 p.m., August 9th and 20th, 1997. The SLICER-measured CHP is the normalized CHP from Fig. 1c.

thickness dh located at height h_i inside the canopy are calculated as:

$$L_{\text{sun}}(h_i) = \frac{\cos(\theta)}{G(\theta)}\left\{\exp\left[-\frac{G(\theta)L_{\text{cum}}(h_{i-1})}{\cos(\theta)}\right] - \exp\left[-\frac{G(\theta)L_{\text{cum}}(h_{i-1})}{\cos(\theta)}\right]\right\},$$
$$L_{\text{shade}}(h_i) = L_{\text{total}} - L_{\text{sun}}(h_i), \quad (7)$$

where $G(\theta)$ is the mean projection of leaf normals on the direction of solar beam (Ross, 1981), $L_{\text{cum}}(h_i)$ is the cumulative LAI of the layers above height h_i, and $L_{\text{total}}(h_i)$ is LAI of the layer at height h_i. Function $G(\theta)$ is 0.5 as for a uniform leaf angular distribution. $L_{\text{cum}}(h_i)$ is calculated as

$$L_{\text{cum}}(h_i) = \sum_{j=1}^{i} F_{\text{a}}(h_j)\cdot\Delta h = \sum_{j=1}^{i}\frac{\text{CHP}(h_i)}{G(\theta)}\Delta h. \quad (8)$$

The total amounts of sunlit and shaded leaves are the same for all three models. As an example, distributions of sunlit and shaded leaves simulated for 2 p.m., August 9th and 20th, 1997, are shown in Fig. 2a,b for the retrieved (Fig. 1c) and the uniform CHPs. A strong dependence on the vertical canopy structure is obvious.

3.3. Leaf photosynthesis

3.3.1. Farquhar's model

The mechanistic model developed by Farquhar et al. (1980) has been most widely used for modeling leaf photosynthesis. Within this model, the instant CO_2 assimilation rate (A_n) of a unit leaf area is calculated as the minimum of the Rubisco-limited rate of ribulose bisphosphate (RuBP) carboxylation,

$$A_c = V_m \frac{C_i - \Gamma^*}{C_i + K_c(1 + P_o/K_o)} - R_d, \tag{9}$$

and the electron transport limited (light-limited) rate of RuBP regeneration,

$$A_j = J \frac{C_i - \Gamma^*}{4.5C_i + 10.5\Gamma^*} - R_d, \tag{10}$$

where V_m is the maximum carboxylation rate (μmol CO_2 m^{-2} s^{-1}); is the internal CO_2 concentration (Pa); $K_c = 30 \cdot 2.1^{(T-25)/10}$ and $K_o = 30{,}000 \cdot 1.2^{(T-25)/10}$ are the Michaelis–Menten constants (Pa) for CO_2 and O_2, respectively, evaluated with air temperature T (°C); $P_o = 0.209P$ is the concentration of O_2 in the atmosphere given that atmospheric pressure $P = 0.103$ MPa and O_2 occupies 20.9% of the air; $\Gamma^* = 0.105 K_c K_o^{-1} P_o$ is the CO_2 compensation point (Pa); J is the electron transport rate (μmol m^{-2} s^{-1}); and $R_d = 0.015 V_m$ is the daytime leaf dark respiration rate.

The maximum rate of carboxylation is a function of temperature and leaf nitrogen content (Bonan, 1995),

$$V_m = V_{m25} 2.4^{(T-25)/10} f(\mathrm{T}) f(\mathrm{Ni}). \tag{11}$$

Here V_{m25} is the value of V_m at 25 °C, which is 33 μmol CO_2 m^{-2} s^{-1} for broadleaf deciduous forests; $f(\mathrm{Ni}) = \mathrm{Ni}/\mathrm{Ni}_{max}$ is a function that adjusts the rate of photosynthesis for foliage nitrogen content (Ni); and f(T) is a function that simulates thermal breakdown of metabolic processes:

$$f(T) = \left\{ 1 + \exp\left[\frac{-220{,}000 + 710(T + 273)}{8.314(T + 273)} \right] \right\}^{-1}. \tag{12}$$

The vertical distribution of Ni within the canopy can be simulated as a simple exponential distribution function

$$N(z) = N_{max} \exp(-z/H), \tag{13}$$

where $N_{max} = 1.5\%$ is the maximum leaf nitrogen at the top of the canopy (see Table 1), z is the distance from the top, and H is the canopy height. We followed the approach used in the WIMOVAC model (Humphries & Long, 1995).

The electron transport rate depends on the photosynthetically active radiation (PAR) absorbed by the leaf and is defined (Farquhar & von Caemmerer, 1982) as

$$J = \frac{J_{max} \mathrm{PAR}}{\mathrm{PAR} + 2.1 J_{max}}, \tag{14}$$

where $J_{max} = 29.1 + 1.64 V_m$ is the light-saturated rate of electron transport (Wullschleger, 1993).

The internal CO_2 concentration, C_i, links to the leaf instant photosynthetic rate as

$$C_i = C_a - P A_n \left(\frac{1.37}{g_b} + \frac{1.65}{g_s} \right), \tag{15}$$

where $C_a = 340 \times 10^{-6}$ P is the ambient CO_2 concentration; g_s is the stomatal conductance (μmol m^{-2} s^{-1}); and g_b is the leaf boundary layer conductance (μmol m^{-2} s^{-1}) (Bonan, 1995). Given g_b, the unit leaf surface area photosynthetic rate can be modeled as a function of stomatal conductance and ambient environmental conditions. Substitution of Eq. (15) into Eqs. (9) and (10) results in quadratic equations for leaf photosynthesis. As an example, instant GPP rates calculated for 2 p.m., August 9th and 20th, 1997, for the retrieved (Fig. 1c) and the uniform CHPs are shown in Fig. 2a,b.

Table 1
Parameters used for photosynthesis modeling

	Value	Unit	Description	Reference
V_{m25}	33	μmol m^{-2} s^{-1}	maximum carboxylation rate at 25 °C	(Bonan, 1995)
Ni_{max}	1.5	%	maximum leaf nitrogen content	(Bonan, 1995)
g_{max}	0.006	m s^{-1}	maximum stomatal conductance	White et al. (2000)
g_{min}	6×10^{-5}	m s^{-1}	minimum stomatal conductance	White et al. (2000)
PAR_{coef}	0.01	μmol m^{-2} s^{-1}	coefficient in the relationship between g_s and PAR	Chen et al. (1999)
T_{opt}	25	°C	optimal temperature	This study
T_{range}	40	°C	maximum temperature range	Chen et al. (1999)
VPD_{open}	1.1	kPa	vapor pressure deficit at stomatal opening	White et al. (2000)
VPD_{close}	3.6	kPa	vapor pressure deficit at stomatal closure	White et al. (2000)
g_b	0.014	m s^{-1}	boundary layer conductance	White et al. (2000)

Conductance units are transformed from (m s^{-1}) into (mol m^{-2} s^{-1}) as g_s (m s^{-1}) = 0.0224 ((273 + T)/273)(P_{st}/P)g_s (mol m^{-2} s^{-2}) (Sellers et al., 1996), where P_{st} is the standard atmospheric pressure.

3.3.2. Stomatal conductance

Leaf stomata perform the conflicting functions of permitting CO_2 to diffuse into a leaf to support photosynthesis and restricting the diffusion of water vapor out of the leaf (Collatz et al., 1991). The optimization of one function necessarily leads to the failure of the other. Generally, it is assumed that stomata try to provide an appropriate balance between the absorption of CO_2 and the restriction of water loss. The complex physiological mechanisms responsible for opening and closing stomata due to changes in environmental conditions are poorly understood. They are sensitive not only to leaf physiological properties, but also to different environmental parameters including the intensity of PAR incident on the leaf surface, leaf temperature, air humidity, concentration of CO_2 in the air, and availability of soil moisture. There is a variety of models predicting stomatal conductance either directly from environmental factors (Running & Coughlan, 1988; Stewart, 1998) or based on studies of the stomatal conductance of leaves (Collatz et al., 1991). In the second case, photosynthetic rate is often used as a variable which makes such a model inapplicable when both conductance and photosynthesis must be calculated.

In this study, stomatal conductance is modeled as a function of three ambient environmental factors including the intensity of PAR, air temperature (T) and vapor pressure deficit (VPD), i.e.,

$$g_s = \max(g_{max} \cdot f(\mathrm{PAR}) \cdot f(T) \cdot (\mathrm{VPD}), g_{min}), \quad (16)$$

where g_{max} is a species-dependent maximum stomatal conductance; g_{min} is the minimum stomatal conductance; and f(PAR), f(T), and f(VPD) are special environmental functions whose values range from 0 to 1 (Jarvis, 1976). This approach was also used by Chen et al. (1999) for their two-leaf model. VPD is calculated from humidity and temperature values (Rosenberg et al., 1983). The scalar functions are modeled as:

$$f(\mathrm{PAR}) = \mathrm{PAR} \cdot \mathrm{PAR}_{coef}/(1 + \mathrm{PAR} \cdot \mathrm{PAR}_{coef}), \quad (17)$$

$$f(\mathrm{T}) = \begin{cases} \ln(T)/\ln(T_{opt}), & T < T_{opt}, \\ \cos(0.5\pi(T - T_{opt})/(T_{range-T_{opt}})), & T \geq T_{opt}, \\ 0, & T < 1, \end{cases} \quad (18)$$

$$f(\mathrm{VPD}) = \begin{cases} 1, & \mathrm{VPD} \leq \mathrm{VPD}_{open}, \\ (\mathrm{VPD}_{close} - \mathrm{VPD})/(\mathrm{VPD}_{close} - \mathrm{VPD}_{open}), & \mathrm{VPD}_{open} < \mathrm{VPD} < \mathrm{VPD}_{close}, \\ 0, & \mathrm{VPD} \geq \mathrm{VPD}_{close}. \end{cases} \quad (19)$$

Short descriptions and values of the parameters in Eqs. (17)–(19) are given in Table 1. Parameter g_{max} establishes the rate of conductance when environmental conditions are non-limiting. Note that g_{min} is not equal to zero. Even when stomata are completely closed, gas exchange still occurs at very low rates through leaf cuticles, which are somewhat leaky to gas exchange (White et al., 2000). Soil moisture availability is not included as an influencing parameter. It is assumed to be optimal.

3.3.3. Boundary layer conductance

Boundary layer conductance, g_b, controls gas diffusion through the stable boundary layer around the leaf surface. Following White et al. (2000), g_b (m s^{-1}) is estimated as

$$g_b = D_{wv}/\delta_{bl}, \quad (20)$$

where D_{wv} is the diffusion coefficient of water vapor in the air, which is 2.4×10^{-5} m^2 s^{-1} at 0.103 MPa and 20 °C, and δ_{bl} (m) is the leaf boundary thickness. Coefficient D_{wv} is assumed to be constant. Thickness δ_{bl} (mm) is a function of wind speed, u (m/s), i.e.,

$$g_{bl} = 4.0(\ell/u)^{1/2}, \quad (21)$$

where ℓ (m) is the leaf length in the wind direction. For a deciduous forest, $\ell = 0.08$ m.

4. Models simulations

Daily GPP rates calculated by the two-leaf model and the coupled model with uniform CHPs were compared with those produced by the coupled model with actual (lidar-retrieved) CHPs over a wide range of environmental conditions and vertical canopy profiles. The analysis was divided into two parts. First, the performances of the models were evaluated as functions of weather conditions. Daily GPP rates were calculated for 100 different profiles (50 measured over the intermediate-aged stand and other 50 measured over the mature stand) for 3 days in August 1997, characterized by different weather patterns. Second, the performances of the models were evaluated as functions of foliage profiles. Daily GPP rates were calculated for one month, August 1997, for three different CHPs. For all three models, photosynthesis was calculated at a half-hour time-step and then integrated over the day-length period defined as in Monteith and Unsworth (1990). Measurements of humidity, temperature, and incident PAR, taken every 3 min, were averaged to produce a 30-min pattern.

4.1. Daily NPP rates as functions of weather conditions

Half-hour variations of temperature, relative humidity and incident direct and diffuse PAR during 3 days chosen for this analysis are shown in Fig. 3. August 9th is a clear day, with relatively high temperature and low humidity. The pattern of diffuse radiation during this day is totally defined by the scattering properties of the atmosphere. The 2 other days are characterized by a different degree of cloudiness. August 12th is a warm day with partial cloud cover and

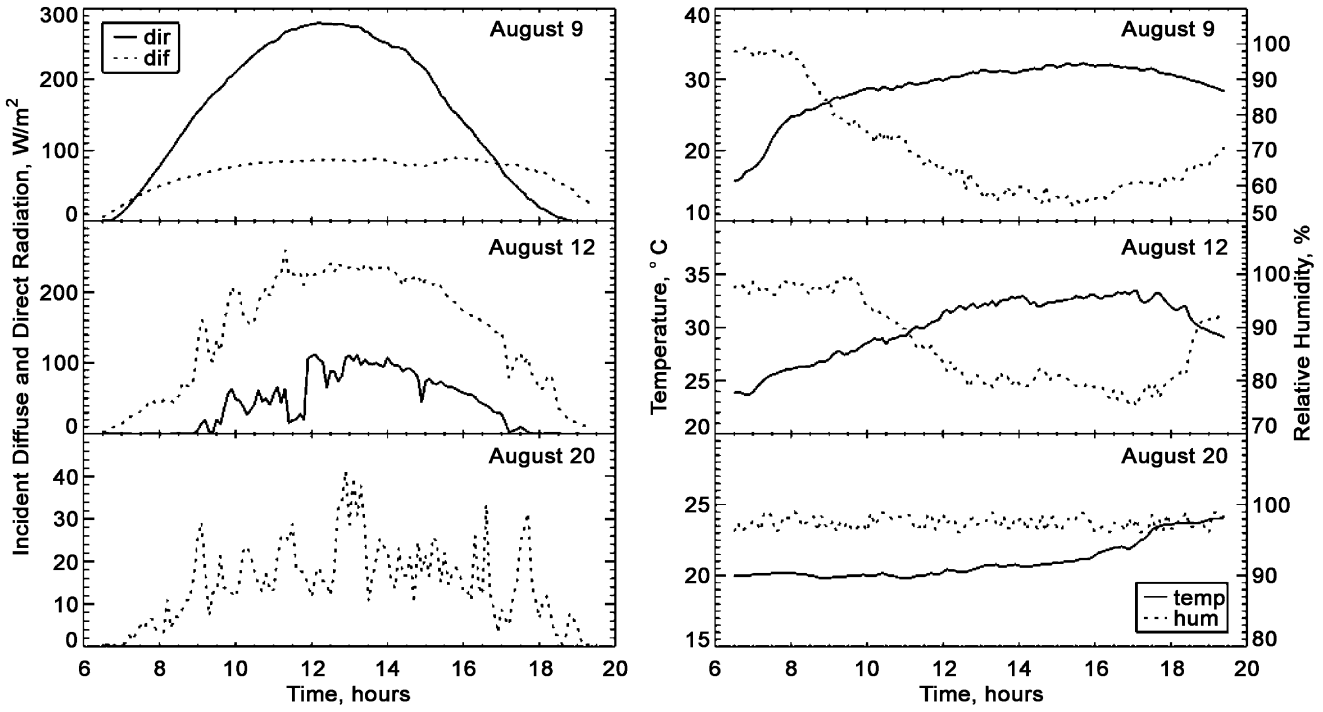

Fig. 3. Daily variations of temperature, humidity and incident PAR for August 9th, 12th, and 20th, 1997. The data were collected at the Wye Research and Education Center (38°55′ N, 76°09′ W) as part of the USDA UV-B Monitoring and Research Program (WWW 1) led by the Natural Research Ecology Laboratory of Colorado State University.

relatively high values of air humidity. August 20th is a cold overcast day with the total amount of direct PAR close to zero. Air humidity on this day varies from 96% to almost 100%. Mean wind speed values are 2.9, 3.1, and 2.7 m s^{-1} for August 9th, 12th, and 20th, respectively.

A frequent time-step in the GPP calculation was necessary to capture the response of photosynthesis to changes in ambient environmental conditions. Sometimes, these changes can be significant. For example, on August 9th, air temperature varies from 15 °C in the early morning to about 32 °C in the afternoon. Several parameters of Farquhar's model, including K_o, K_c, Γ, and V_m, are highly sensitive to such temperature variations. Their non-linear response to temperature changes causes a non-linear response in photosynthesis. Ignoring these variations, e.g., using mean daily values of temperature, may lead to large errors in calculated daily GPP rates.

The results of simulations are represented in Fig. 4 for the coupled model with uniform and actual CHPs and in Table 2 for the two-leaf model and the coupled model with actual CHPs. A different presentation pattern is used as the two-leaf model does not account for variations of CHPs. Its simulations depend only on the total LAI values of sunlit and shaded leaves, which, in our study, were the same for 50 intermediate-stand and 50 mature-stand profiles.

Let consider Fig. 4 first. We applied the following classification to distinguish between CHPs. The profiles were divided into four groups: (1) CHPs with more than 80% of foliage concentrated in the upper two-thirds of the tree height, (2) CHPs with more than 80% of foliage in the lower two-thirds of the tree; (3) approximately uniform CHPs; (4) remaining CHPs. As seen in Fig. 4a, the intermediate stand does not have any uniform profiles. The first group is dominant. For the mature stand, some uniform CHPs are present. In general, this stand is characterized by a more random distribution of canopy material.

The shape of a SLICER waveform and, therefore, the CHP retrieved from it, changes dramatically in a set of measurements for the same site. It depends on the number of factors including the density of vegetation, shape of the canopy, number of trees within the footprint, canopy height variance, and roughness of the ground surface. Given a SLICER waveform, it is impossible to say from which of the two stands it comes from, if these stands are characterized by the same average tree height. However, the analysis of a range of signals measured over the stands can reveal some of the differences.

The plots in Fig. 4 show that the use of a uniform foliage profile instead of the actual one leads sometimes to large differences in the calculated GPP values. For the intermediate stand, the difference is larger for the profiles with more than 80% of foliage concentrated in the upper two-thirds of the height. Such dependence on the foliage profile is not observed for the mature stand. For this stand, profiles with the largest differences are representatives of the fourth

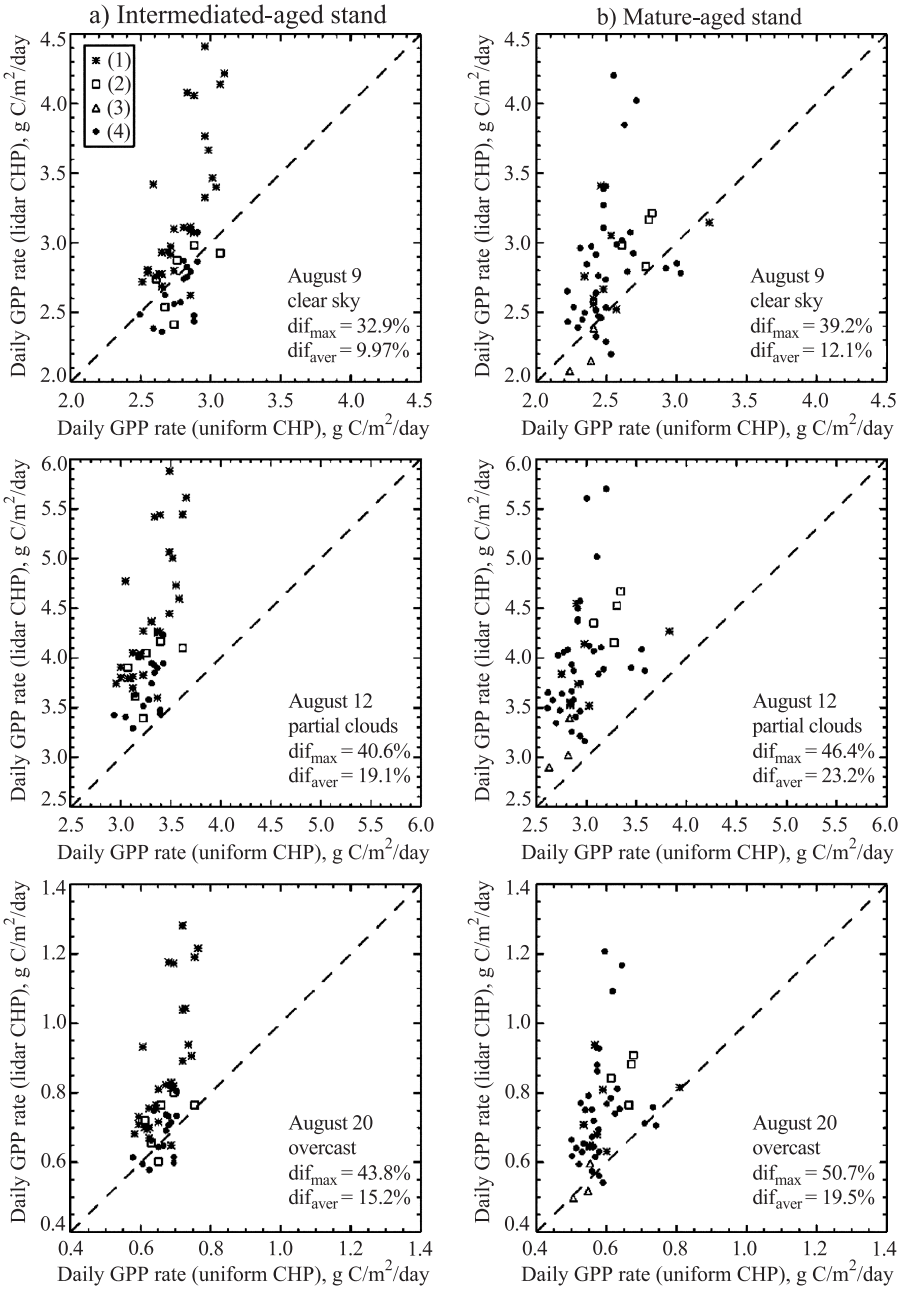

Fig. 4. Agreement between daily GPP rates estimated by the coupled model with actual (lidar-measured) and uniform CHPs. The left panel shows the simulations for the intermediate-aged stand. The right panel shows the simulations for the mature stand. GPP rates are calculated for 3 days with different weather conditions. CHPs are classified into four groups: (1) more than 80% of foliage is concentrated in the upper two-thirds of the canopy height; (2) more than 80% of foliage in the lower two-thirds; (3) approximately uniform; (4) not suitable for the first three groups.

classification group. However, profiles classified as not suitable to the first three groups may still be really close to either of them.

In general, the mature stand is characterized by slightly higher values of average and maximum differences for all 3 days. We suspect that it might be related to a larger value of the average LAI, 5.26 versus 5.16 for the intermediate stand.

The best agreement is observed for August 9th, for both the intermediate and the mature stands. The averages differences between the models simulations do not exceed 13%. However, the maximum possible differences are still high, more than 30% for the both stands. August 12th and August 20th are characterized by a worse agreement between the calculated GPP rates. The average differences are a little higher for August 12th than for August 20th, while the maximum observed differences are higher for August 20th, for the both stands.

During clear sky days, the fraction of diffuse radiation incident on the leaves is relatively low and originates

Table 2
The results of the comparison between daily GPP rates calculated by the two-leaf model and the coupled model with actual CHPs

	Forest stand	August 9 (clear sky)	August 12 (partial clouds)	August 20 (overcast)
Daily GPP rate ($gC\ m^{-2}\ day^{-1}$)	intermediate	2.987	3.167	0.516
	mature	2.994	3.172	0.515
Average difference with the coupled model (%)	intermediate	11.9	21.7	32.2
	mature	13.9	18.2	28.3
Maximum difference with the coupled model (%)	intermediate	32.3	46.1	59.7
	mature	44.0	44.3	57.3

The comparison was performed for 3 days with different weather conditions for the intermediate-aged and the mature stands.

mostly from the scattering of a direct solar beam inside the canopy rather than from its scattering in the atmosphere. The CO_2 assimilation rate of shaded leaves is limited by the light availability and strongly depends on the amount of diffuse PAR incident on their surfaces. In the contrary, sunlit leaves have enough irradiance and their photosynthesis is controlled by the Rubisco activity. The contribution of sunlit leaves into the total canopy GPP rate is higher than that of shaded leaves. Good agreement is observed between the simulations with uniform and actual CHPs because, in this case, this is the total amount of foliage that matters. However, the concentration of foliage in the upper part of the tree causes more intensive scattering of direct radiation. The contribution of shaded leaves becomes more significant. The coupled model with actual CHPs, capable to account for these changes, provides higher values of daily GPP rates.

During the days with partial and total cloud cover, photosynthesis is mostly controlled by the amount of PAR incident on the leaves surfaces. In this case, the distribution of radiation inside the canopy plays an important role. Differences in the radiation distribution patterns lead to further differences in the photosynthetic rates.

Note that the calculated GPP rates are higher for August 12th compared to August 9th. The obtained results correlate with those described in Gu et al. (2002), who studied the influence of diffuse radiation on canopy photosynthesis. The increased diffuse radiation from the sky is likely to enhance the carbon assimilation process but, of course, it is not the only factor responsible for this enhancement. The presence of clouds leads to changes in air temperature, VPD and soil moisture, which result in further changes in the CO_2 assimilation rate.

The similar situation is observed for the two-leaf model (Table 2). Daily GPP rates calculated for August 12th are higher than those calculated for August 12th. In general, this model demonstrates almost the same disagreement pattern with the coupled model with actual CHPs as the coupled model with uniform profiles, for August 9th and August 12th. We think this is reasonable as the empirical equations for the two-leaf model were developed based on the assumption of a uniform vertical distribution of leaves. Disagreement becomes larger for August 20th, but not too much.

4.2. Daily NPP rates as functions of foliage profiles

Three different CHPs used in this analysis are shown in Fig. 5. They were selected to reflect variability of foliage distributions: majority of the foliage concentrated in the first half of the canopy; a nearly uniform distribution; majority of the foliage in the lower half of the canopy.

Day-to-day variations of the environmental parameters used in photosynthesis calculation are shown in Fig. 6. Relatively large variations of all parameters are evident. Mean daily temperature varies from the maximum of 38 °C on August 17th to the minimum of 23 °C on August 20th, which is the coolest day of this month. Humidity ranges from approximately 72% for sunny days to 98% for cloudy days. Variation of daily mean incident direct and diffuse PAR is a general indicator of the degree of cloudiness. For overcast days, such as August 20th and 31st, the amount of direct PAR is almost zero.

The results of daily GPP calculations are shown in Fig. 7. All three models demonstrate a similar response to the changes in weather conditions. For overcast days, like days 20, 29, 30, and 31, photosynthesis activity is sharply reduced, due to the light insufficiency. Clouds can increase the amount of diffuse radiation incident on the ground only if the sky is not too cloudy. Increased diffuse radiation can enhance ecosystem carbon assimilation (Gu et al., 2002). For example, days 3, 11–13, and 25–28, when the amounts of incident diffuse radiation were high, are characterized by higher photosynthesis activity than days 1, 9, 16, and 17,

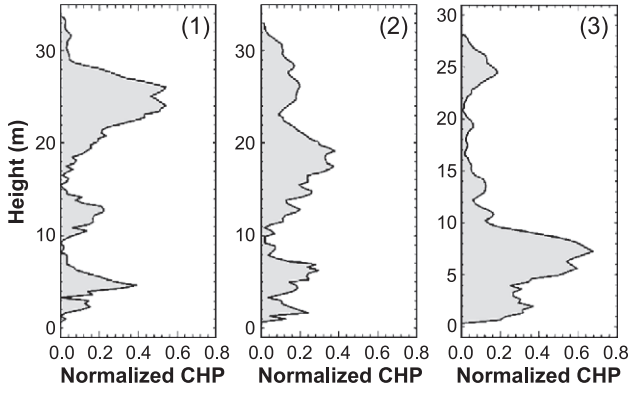

Fig. 5. Three different CHPs retrieved from SLICER waveforms. The profiles were selected to reflect the variability of foliage distributions: majority of the foliage concentrated in the first half of the canopy; a nearly uniform distribution; majority of the foliage in the lower part of the canopy. The third CHP is the normalized CHP from Fig. 1c. Total CAI for all three profiles is 5.26.

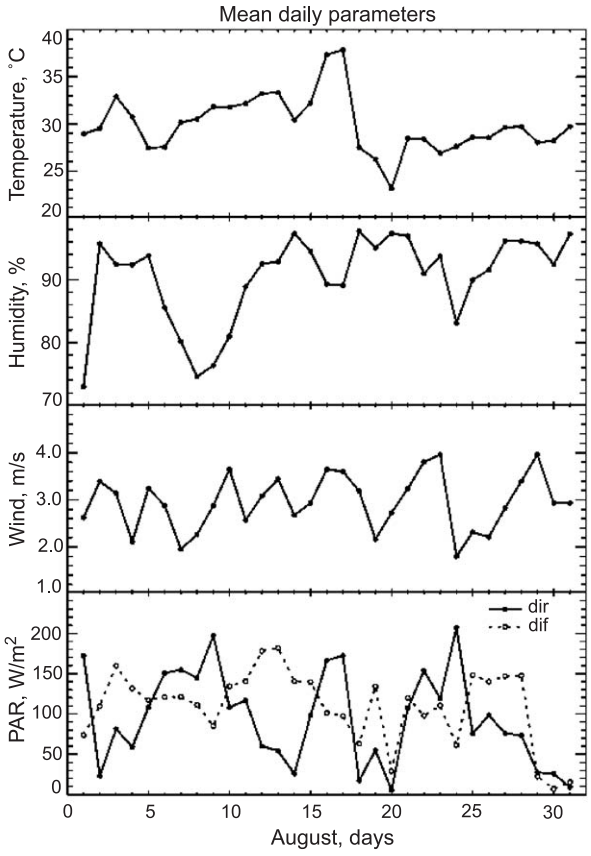

Fig. 6. Mean daily environmental parameters for August 1997. Incident radiation, temperature, and humidity were measured at 3-min time-step at the Wye Research and Education Center (38°55′ N, 76°09′ W), as part of the USDA UV-B Monitoring and Research Program (WWW 1). Daily mean wind speed values were collected at the Andrews AFB station (38°49′ N, 76°52′ W), (WWW 2).

with clear sky conditions and larger portions of incident direct PAR. Even though the average air temperature for day 17 is the highest of the month, its carbon assimilation rate is relatively low.

Both the two-leaf model and the coupled model with uniform CHPs demonstrate the worst agreement with the coupled model with actual CHPs for the first profile in Fig. 5. The average difference is 23.6% for the two-leaf model and 32.9% for the coupled model with uniform CHPs. The use of the uniform profile results in a stable relative underestimation of canopy photosynthesis. The underestimation is a little smaller for the clear warm days, such as 1, 9, 16, 17, and 24, but, in general, it slightly varies around its average value. We suggest that this underestimation is associated not only with the differences in the radiation distribution pattern but also with the differences in the amounts of leaves contributing into the total canopy photosynthesis. For the uniform profile, the contribution of leaves located between the ground and one third of the tree height is almost negligible (See Fig. 2). For the actual profile, the contribution of such leaves is also negligible but the amount of foliage concentrating in the upper part of the tree is much higher than that for the uniform profile.

The agreement between the coupled model with actual CHPs and the two other models is also not satisfactory for the third profile from Fig. 5. The average difference is 21.9% for the two-leaf model and 20.5% for the coupled model with uniform CHPs. However, the both models provide almost the same estimates of daily GPP rates. The clear sky days, such as 1, 9, 16, 17, and 24, are characterized by smaller differences with the coupled model with actual CHPs. The discrepancy range does not exceed 7%. The differences exceed the average values for the days with partial cloud cover, such as 3–7, 10–15, and 25–28. A large relative underestimation of the GPP rates is evident. The underlying mechanisms responsible for these differences are the same as for the first profile in Fig. 5. The amount of foliage contributing significantly to photosynthesis is higher for the actual profile than for the uniform. The third profile is almost a "reflection" of the first profile with respect to the middle of the tree height.

The best agreement is observed for the second profile from Fig. 5, which is close to uniform. The average difference between the coupled models with uniform and actual CHPs does not exceed 8%. In general, the difference is small for all days except for days 29, 30, and 31, when it is 19.3%, 44.6%, and 19.7%, respectively. A question arises why this effect is not observed for day 20. For this day, the difference between the two models simulations is only 2.1%. We suspect this is related to the fact that the total amount of direct PAR for this day is almost 0. For days 29, 30, and 31 the production of sunlit leaves increases rapidly during short periods when a sun beam appears from the clouds. As the performance of the coupled model is extremely sensitive to the distribution of PAR inside the canopy, slight differences in the irradiances of sunlit leaves, caused by the use of different CHPs, lead to large differences in GPP rates.

The behavior of the two-leaf model for this profile is slightly different. Large differences (more than 25%) with the coupled model with actual CHPs are observed not only for the last 3 days of the month, but also for the days with clear sky conditions, including 1, 9, 16, 17, and 24. For clear sky days, the two-leaf model always relatively overestimates the contribution of sunlit leaves, compared to the coupled model.

5. Sensitivity study

Large differences between the daily GPP rates calculated by the two-leaf model and the coupled model with actual CHPs may give a wrong impression about the two-leaf model performance. It is important to evaluate these two models on the same basis, i.e., when the average rates of PAR absorption

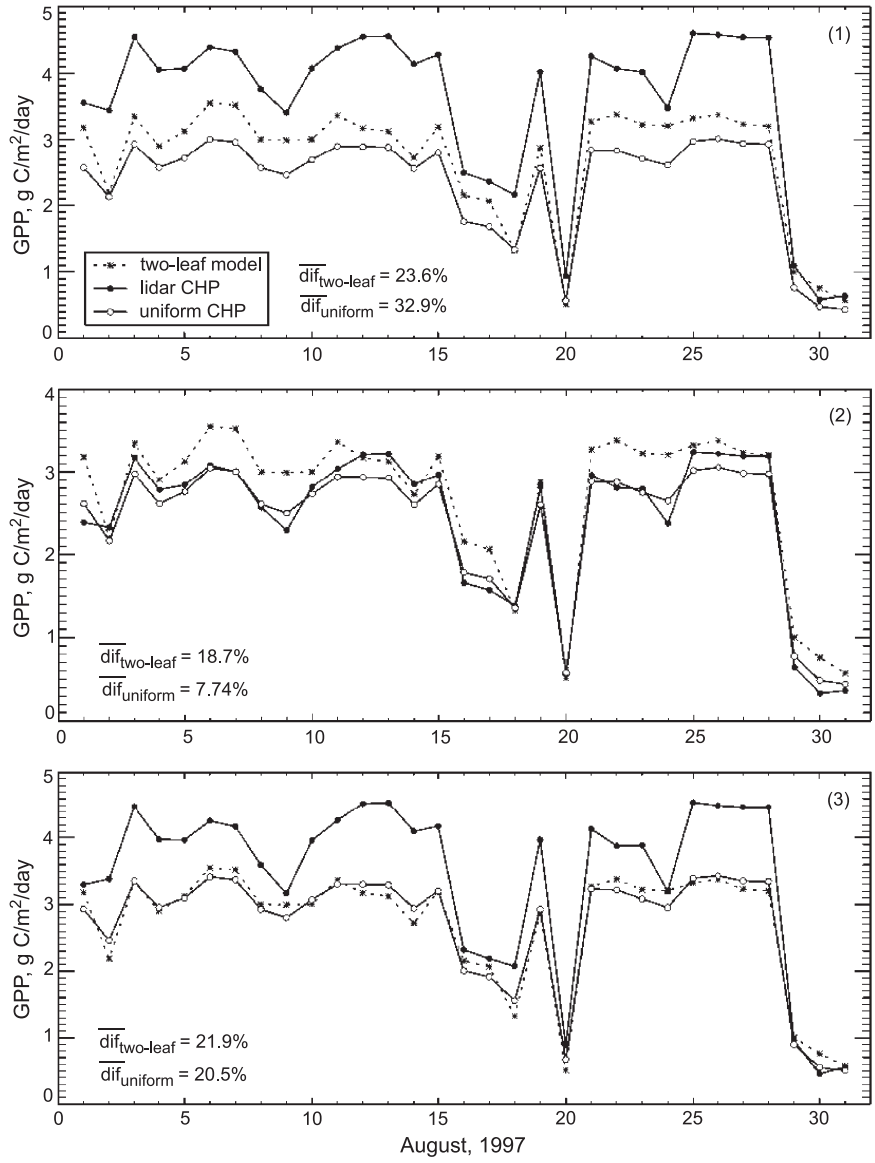

Fig. 7. Variations of daily GPP rates calculated by the coupled model with actual and uniform CHPs and the two-leaf model for the three CHPs shown in Fig. 5. Calculations are made for August 1997.

for sunlit ($\bar{S}_{sun}$) and shaded ($\bar{S}_{shade}$) leaves are similar. For each time step, these average rates are calculated as

$$\bar{S}_{sun} = \frac{\sum_{i=1}^{N}(S_{dir}(i) + S_{dif}(i)) \cdot L_{sun}(i)}{\sum_{i=1}^{N} L_{sun}(i)}, \quad (22)$$

and

$$\bar{S}_{shade} = \frac{\sum_{i=1}^{N} S_{dif}(i) \cdot L_{shade}(i)}{\sum_{i=1}^{N} L_{shade}(i)}, \quad (23)$$

where S_{dif} and $S_{dir}$are the amounts of the diffuse and direct PAR absorbed in each layer; L_{sun} and L_{shade} are the sunlit and shaded leaves LAI.

$\bar{S}_{sun}$ and $\bar{S}_{shade}$ were calculated for each CHP from the intermediate-aged stand and then incorporated into the two-leaf model. Under such an approach, the total amounts of PAR absorbed by the sunlit and shaded leaves were approximately the same. The results are represented in Table 3. The differences in the calculated daily GPP rates became much smaller. The average difference for all 3 days does not exceed 5%.

The performance of the two-leaf model is extremely sensitive to the selection of the radiation pattern. In Eqs. (5) and (6), which are typically used in the two-leaf models, fifty different CHPs were treated as the same. The use of

Table 3
The results of the sensitivity study for the two-leaf model

Daily GPP rates	August 9 (clear sky)	August 12 (partial clouds)	August 20 (overcast)
Max difference (%)	7.5	9.9	2.4
Average difference (%)	3.5	5.0	0.7

Daily GPP rates were calculated for 50 intermediate stand CHPs by the two-leaf model and the coupled model with actual CHPs under the same average rate of PAR absorption for sunlit and shaded leaves.

different radiation pattern to calculate the absorbed PAR was the main reason of the large differences between the two-leaf and the coupled model. One way to reduce these differences is to develop new equations, which will account for variations in the vertical distribution of foliage.

6. Conclusions

The performances of three canopy photosynthesis models utilizing different types of foliage representation were compared in this study over a wide range of vertical foliage distributions and weather conditions. A conclusion is made that the account of actual foliage profiles is significant for estimation of canopy photosynthesis. It allows for capturing the distribution of incident direct and diffuse PAR as well as the distribution of sunlit and shaded leaves inside the canopy. This might lead to more accurate estimates of daily GPP rates in photosynthesis models, which rely on the extrapolation of Farquhar's model from a unit leaf area to the whole canopy. We did not make a comparison with experimental estimates of GPP as they were not available for the SERC study site. However, the maximum obtained difference between the simulations with uniform and actual foliage profiles (46.4% and 50.7% for the days with partial and total cloud cover) are large enough to demonstrate the importance of the accounting for vertical foliage structure.

The obtained results showed that the disagreement range was almost the same for the two-leaf model and the coupled model with uniform CHPs. This means that it might be useless to apply a multiple layer division in addition to the two-leaf separation if the actual foliage profile is not known. A multiple layer modeling is important to capture the radiation distribution inside the canopy but, if it were possible to develop equations that evaluate average absorbed PAR for different foliage profiles with great accuracy, the multiple layer division would be unnecessary. Besides, compared to the coupled model, the two-leaf model has an advantage of being simple enough to be incorporated in large-scale models. The coupled model is computationally much more expensive.

Several important issues related to the retrieval of CHPs need to be emphasized. First, a CHP was used as a substitute for the actual foliage profile. We assume that the influence of non-foliated surfaces in the retrieved waveforms is negligible. Unfortunately, this assumption is a part of every research associated with CHPs. Second, CHPs were retrieved under the assumption of single-scattering. The effects of multiple scattering are mostly related to an enhancement of the lower part of the signal; ignoring multiple scattering leads to an erroneous assignment of a larger amount of foliage to the lower part of the canopy (Kotchenova et al., 2003). Third, CHPs were retrieved under the assumption of a uniform horizontal distribution of leaves. We ignored the influence of foliage clumping. And, fourth, the retrieved CHPs were normalized with average field estimates of LAI. The normalization with location-specific estimates of LAI would be more accurate but such measurements were not available. However, all these issues should not be considered critical for the analysis performed here as we did not make a comparison with experimentally measured rates of photosynthesis.

In general, forest CHPs can be largely diverse over relatively small areas (Lefsky et al., 1999). Measuring just a few typical profiles from the ground will not capture the real vertical heterogeneity of forest structure. Vegetation canopy lidars facilitate rapid measurement of canopy height profiles over relatively large regions. The leaf-separation/multilayer model with lidar-measured CHPs, developed in this study, can, therefore, be applied at local and regional scales.

Besides the importance of vertical foliage profiles, this study also demonstrates the importance of separate measurements of diffuse and direct radiation. We did not address directly the canopy photosynthesis differences between diffuse and direct radiation, but we showed that a certain increase in the incident diffuse PAR due to partial cloudiness could significantly enhance the daily carbon assimilation rate. Currently, only total incident PAR is measured by most flux towers and meteorological stations. This practice hampers theoretical and experimental studies of the influence of diffuse radiation on canopy photosynthesis. Separate routine measurements of diffuse and direct radiation are as important as measurements of other environmental parameters.

Acknowledgements

The authors would like to thank David Harding and Kathy Still for providing the SLICER data. They would also like to thank Nathan Phillips and four anonymous reviewers for helpful comments. This work was supported by NASA Headquarters under the Earth System Science Fellowship grant NGT5-30462.

Appendix A. Calculation of FHP

Ni-Meister et al. (2001) used FHP as a substitution of CHP. For CHP, Eq. (1) is written as

$$\mathrm{CHP}_{\mathrm{retr}}(z) = \mathrm{CHP}_{\mathrm{act}}(z) \cdot G(z, \theta_{\mathrm{L}}), \tag{A1}$$

where $CHP_{retr}(z)$ is the CHP retrieved with the help of MacArthur and Horn's method and $CHP_{act}(z)$ is the actual canopy profile.

To get a relative CHP ($CHP_{rel}(z)$), with the CAI scaled to 1, one needs to divide $CHP_{act}(z)$by the total cumulative canopy area index, i.e.,

$$CHP_{rel}(z) = (CHP_{retr}(z)/G(z,\theta_L))/CAI_{act}, \quad (A2)$$

$$\text{where } CAI_{act} = \sum_{z}^{H} CHP_{act}(z) \cdot dz. \quad (A3)$$

To extract the actual distribution of foliage, we normalized the relative CHPs with the ground-measured LAIs, i.e.,

$$FHP(z) = CHP_{rel}(z) \cdot LAI. \quad (A4)$$

If we assume that $G(z,\theta_L)$ is constant through the whole canopy and does not depend on z, then

$$FHP(z) = (CHP_{retr}(z)/CAI_{retr}) \cdot LAI. \quad (A5)$$

Appendix B. WWW sites

WWW 1: Wye Research and Education Center data, http://uvb.nrel.colostate.edu/UVB/uvb_climate_network.html.

WWW 2: Andrews AFB station data, http://www.ncdc.noaa.gov/oa/climate/onlineprod/drought/xmgr.html.

References

Blair, J. B., Rabine, D. L., & Hofton, M. A. (1999). The laser vegetation imaging sensor: A medium-altitude, digitisation-only, airborne laser altimeter for mapping vegetation and topography. *ISPRS Journal of Photogrammetry and Remote Sensing*, *54*, 115–122.

Bonan, G. B. (1995). Land-atmosphere CO_2 exchange simulated by a land surface process model coupled to an atmospheric general circulation model. *Journal of Geophysical Research*, *100*(D2), 2817–2831.

Chen, J. M., Liu, J., Cihlar, J., & Goulden, M. L. (1999). Daily canopy photosynthesis model through temporal and spatial scaling for remote sensing applications. *Ecological Modelling*, *124*, 99–119.

Chen, J. M., Rich, P. M., Gower, S. T., Norman, J. M., & Plummer, S. (1997). Leaf area index of boreal forests: Theory, techniques, and measurements. *Journal of Geophysical Research*, *102*(D24), 29429–29443.

Collatz, G. L., Ball, J. T., Crivet, C., & Berry, J. A. (1991). Physiological and environmental regulation of stomatal conductance, photosynthesis and transpiration: A model that includes a laminar boundary layer. *Agricultural and Forest Meteorology*, *54*, 107–136.

De Pury, D. G. G., & Farquhar, G. D. (1997). Simple scaling of photosynthesis from leaves to canopies without the errors of big-leaf models. *Plant, Cell & Environment*, *20*, 537–557.

De Pury, D. G. G., & Farquhar, G. D. (1999). A commentary on the use of a sun/shade model to scale from the leaf to canopy. *Agricultural and Forest Meteorology*, *95*, 257–260.

Drake, J. B., Dubayah, R., Knox, R. G., Clark, D. B., & Blair, J. B. (2002). Sensitivity of large-footprint lidar to canopy structure and biomass in a neotropical forest. *Remote Sensing of Environment*, *81*, 378–392.

Farquhar, G. D., & Roderick, M. L. (2003). Pinatubo, diffuse light and the carbon cycle. *Science*, *229*, 1997–1998.

Farquhar, G. D., & von Caemmerer, S. (1982). Modelling of photosynthetic response to environmental conditions. In O. L. Lange, P. S. Nobel, C. B. Osmond, & H. Ziegler Jr. (Eds.), *Encyclopedia of Plant Physiology, New Series: Physiological Plant Ecology II*, *vol. 12B* (pp. 549–587). Berlin: Spring Verlag.

Farquhar, G. D., von Caemmerer, S., & Berry, J. A. (1980). A biochemical model of photosynthetic CO_2 assimilation in leaves of C_3 species. *Planta*, *149*, 78–90.

Gu, L., Baldocchi, D., Verma, S. B., Black, T. A., Vesala, T., Falge, E. V., & Dowty, P. R. (2002). Advantages of diffuse radiation for terrestrial ecosystem productivity. *Journal of Geophysical Research*, *107*(D6) (10.1029/2001JD001242). ACL (2), 1–23.

Guenther, A., Hewitt, C. N., Erickson, D., Fall, R., Geron, C., Graedel, T., Harley, P., Klinger, L., Lerdau, M., McKay, W. A., Pierce, T., Schoels, B., Steinbrecher, R., Tallamraju, R., Taylor, J., & Zimmerman, P. (1995). A global model of natural votalite organic compound emissions. *Journal of Geophysical Research*, *100*(D5), 8873–8892.

Harding, D. J., Blair, J. B., Rabine, D. L., & Still, K. L. (2000). SLICER airborne laser altimeter characterization of canopy structure and sub-canopy topography for the BOREAS northern and southern study regions: Instrument and data product description. In F. G., Hall, & J., Nickeson, (Eds.), Technical report series on the Boreal Ecosystem-Atmospheric Study (BOREAS). Washington, DC: NASA/TM-2000-209891.

Harding, D. J., Lefsky, M. A., Parker, G. G., & Blair, J. B. (2001). Laser altimeter canopy height profiles, methods and validation for closed-canopy, broadleaf forests. *Remote Sensing of Environment*, *76*, 283–297.

Harrison, L., Michalsky, J., & Berndt, J. (1994). Automated multifilter rotated shadow-based radiometer: An instrument for optical depth and radiation measurements. *Applied Optics*, *33*(22), 5118–5125.

Heinsch, F. A., Reeves, M., Bowker, C. F., Votava, P., Kang, S., Milesi, C., Zhao, M., Glassy, J., Jolly, W. M., Kimball, J. S., Nemani, R. R., & Running, S. W. (2003). User's Guide, GPP and NPP (MOD17A2/A3), NASA MODIS Land Algorithm, Version 1.2. www.ntsg.umt.edu/modis/MOD17UsersGuide.pdf.

Humphries, S. W., & Long, S. P. (1995). WIMOVAC—A software package for modeling the dynamics of plant leaf and canopy photosynthesis. *Computer Applications in the Biosciences*, *11*(4), 361–371.

Hunt, E. R., Piper, S. C., Nemani, R. R., Keeling, C. D., Otto, R. D., & Running, S. W. (1996). Global net carbon exchange and intra-annual atmospheric CO_2 concentrations predicted by an ecosystem simulation model and three-dimensional atmospheric transport model. *Global Biogeochemical Cycles*, *10*, 431–456.

Intergovernmental Panel on Climate Change (2001). Chap. 3—The carbon cycle and atmospheric carbon dioxide. *Climate Change 2001: The scientific basis*. Cambridge, UK: Cambridge University Press.

Jarvis, P. G. (1976). The interpretation of leaf water potential and stomatal conductance found in canopies in the field. *Philosophical Transactions of the Royal Society of London. Series B*, *273*, 593–610.

Kotchenova, S. Y., Shabanov, N. V., Knyazikhin, Y., Davis, A. B., Dubayah, R., & Myneni, R. B. (2003). Modeling lidar waveforms with time-dependent stochastic radiative transfer theory for remote estimations of forest structure. *Journal of Geophysical Research*, *108*(D15), 4484 (10.1029/2002JD003288).

Lefsky, M. A., Cohen, W. B., Acker, S. A., Parker, G. G., Spies, T. A., & Harding, D. (1999). Lidar remote sensing of the canopy structure and biophysical properties of Douglas-fir western hemlock forests. *Remote Sensing of Environment*, *70*, 339–361.

Lefsky, M. A., Harding, D. J., Cohen, W. B., Parker, G. G., & Shugart, H. H. (1999). Surface lidar remote sensing of basal area and biomass in deciduous forests of eastern Maryland, USA. *Remote Sensing of Environment*, *67*, 83–98.

MacArthur, R. H., & Horn, H. C. (1969). Foliage profiles by vertical measurements. *Ecology*, *50*, 802–804.

Monteith, J. L., & Unsworth, M. H. (1990). *Principles of environmental physics* (2nd ed.) (p. 10) London: Edward Arnold.

Ni-Meister, W., Jupp, D. L. B., & Dubayah, R. (2001). Modeling lidar waveforms in heterogeneous and discrete canopies. *IEEE Transactions on Geoscience and Remote Sensing*, *39*(9), 1943–1958.

Norman, J. M. (1980). Interfacing leaf and canopy light interception models. In J. D. Hesketh, & J. W. Jones (Eds.), *Predicting Photosynthesis for Ecosystem Models, vol. II* (pp. 49–67). Boca Raton, FL: CRC Press.

Parker, G. G., Lefsky, M. A., & Harding, D. J. (2001). Light transmittance in forest canopies determined using airborne laser altimetry and in-canopy quantum measurements. *Remote Sensing of Environment*, *73*, 298–310.

Potter, C. S., Randerson, J. T., Field, C. B., Matson, P. A., Vitousek, P. M., Mooney, H. A., & Klooster, S. A. (1993). Terrestrial ecosystem production: A process model based on global satellite and surface data. *Global Biogeochemical Cycles*, *7*, 811–841.

Rosenberg, N. J., Blad, B. L., & Verma, S. B. (1983). *Microclimate: The biological environment, vol. 170* (2nd ed.) (pp. 13–15). New York: John Wiley & Sons.

Ross, J. (1981). The radiation regime and architecture of plant stands. Hague, Netherlands: Dr. Junk Publishers.

Ruimy, A., Dedieu, G., & Saugier, B. (1996). TURC: A diagnostic model of continental gross primary productivity and net primary productivity. *Global Biochemical Cycles*, *10*, 269–285.

Running, S. W., & Coughlan, J. C. (1988). A general model of forest ecosystem processes for regional application: I. Hydrological balance, canopy gas exchange and primary production processes. *Ecological Modelling*, *42*, 125–154.

Sellers, P. J., Berry, J. A., Collatz, G. J., Field, C. B., & Hall, F. G. (1992). Canopy reflectance, photosynthesis and transpiration: III. A reanalysis using improved leaf models and a new canopy integration scheme. *Remote Sensing of Environment*, *42*, 187–216.

Sellers, P. J., Randall, D. A., Collatz, G. J., Berry, J. A., Field, C. B., Dazlich, D. A., Zhang, C., Collelo, G. D., & Bounoua, L. (1996). A revised land surface parameterization (SiB_2) for atmospheric GCMs: Part I. Model Formulation. *Journal of Climate*, *9*, 676–705.

Shabanov, N. V., Knyazikhin, Y., Baret, F., & Myneni, R. B. (2000). Stochastic modeling of radiation regime in discontinuous vegetation canopies. *Remote Sensing of Environment*, *74*, 125–144.

Shabanov, N. V., Wang, Y., Buermann, W., Dong, J., Hoffman, S., Smith, G. R., Tian, Y., Knyazikhin, Y., & Myneni, R. B. (2003). Effect of foliage spatial heterogeneity on the MODIS LAI and FPAR algorithm over broadleaf forests. *Remote Sensing of Environment*, *85*, 410–423.

Spitters, C. J. T. (1986). Separating the diffuse and direct components of global radiation and its implications for modeling canopy photosynthesis: Part II. Calculation of canopy photosynthesis. *Agricultural and Forest Meteorology*, *38*, 231–242.

Stewart, J. B. (1998). Modeling surface conductance of pine forests. *Agricultural and Forest Meteorology*, *43*, 19–35.

Wang, Y. P., & Leuning, R. (1998). A two-leaf model for canopy conductance, photosynthesis and partitioning of available energy: I. Model description and comparison with a multi-layered model. *Agricultural and Forest Meteorology*, *91*, 89–111.

White, M. A., Thornton, P. E., Running, S. W., & Nemani, R. R. (2000). Parameterization and sensitivity analysis of the BIOME-BGC terrestrial ecosystem model: net primary production controls. *Earth Interactions*, *4*(3), 1–85.

Wullschleger, S. D. (1993). Biochemical limitations to carbon assimilation in C_3 plants—A retrospective analysis of the A/C_i curves from 109 species. *Journal of Experimental Botany*, *44*, 907–920.

Zwally, H. J., Schutz, B., Abdalati, W., Abshire, J., Bentley, C., Brenner, A., Bufton, J., Dezio, J., Hancock, D., Harding, D., Herring, T., Minster, B., Quinn, K., Palm, S., Spinhirne, J., & Thomas, R. (2002). ICESat's laser measurements of polar ice, atmosphere, ocean and land. *Journal of Geodynamics*, *34*, 405–445.